Efficient Numerical Simulations Using Matrix-Product States

Frank Pollmann
frankp@pks.mpg.de

Max-Planck-Institut für Physik komplexer Systeme,
01187 Dresden, Germany

September 13, 2015

[see Ref. 8 for a complete list of relevant literature]

1 Entanglement in quantum-many body systems

Entanglement is one of the fundamental phenomena in quantum mechanics and implies that different degrees of freedom of a quantum system cannot be described independently. Over the past decades it was realized that the entanglement in quantum many-body system can give access to a lot of useful information about quantum states. First, entanglement related quantities provide powerful tools to extract universal properties of quantum states. For example, scaling properties of the entanglement entropy help to characterize critical systems [1, 2, 3, 4], and entanglement is the basis for the classification of topological orders [5, 6]. Second, the understanding of entanglement helped to develop new numerical methods to efficiently simulate quantum many-body systems [7, 8]. In the following, we give a short introduction to entanglement in 1D systems and then focus on the MPS representation.

Let us consider the bipartition of the Hilbert space $\mathcal{H} = \mathcal{H}_L \otimes \mathcal{H}_R$ of a 1D system as illustrated in Fig. 1(a), where $\mathcal{H}_L$ ($\mathcal{H}_R$) describes all the states defined on the left (right) of a given bond. In the so called *Schmidt*

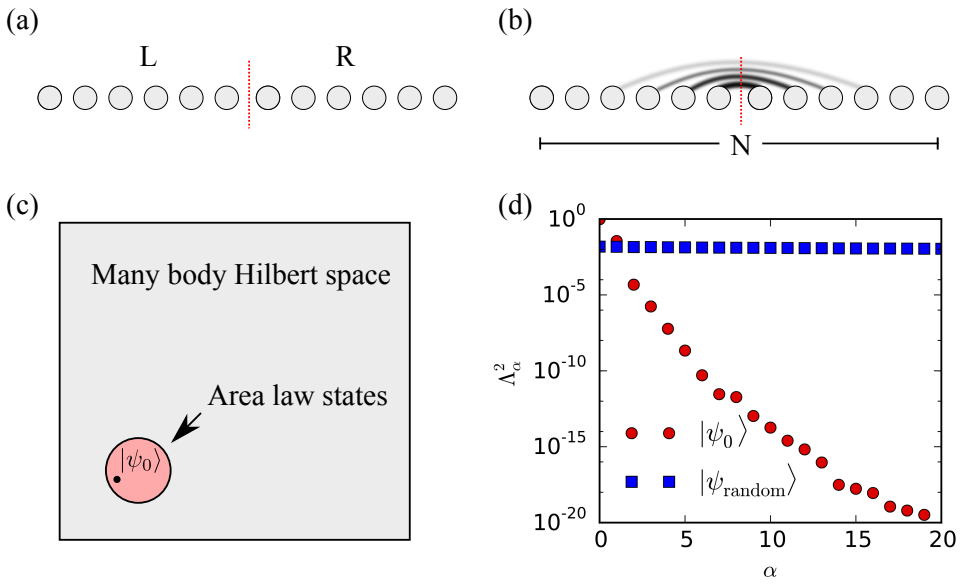

Figure 1: (a): Bipartition of a 1D system into two half chains. (b): Significant quantum fluctuations in gapped ground states occur only on short length scales. (c): 1D area law states make up a very small fraction of the many-body Hilbert space but contain all gapped ground states. (d): Comparison of the entanglement spectrum of the ground state of the transverse field Ising model ($g = 1.5$) and a random state for a system consisting of $N = 16$ spins.

decomposition, a state $|\Psi\rangle \in \mathcal{H}$ is decomposed as

$$|\Psi\rangle = \sum_\alpha \Lambda_\alpha |\alpha\rangle_L \otimes |\alpha\rangle_R, \quad |\alpha\rangle_{L(R)} \in \mathcal{H}_{L(R)}, \tag{1}$$

where the states $\{|\alpha\rangle_{L(R)}\}$ form an orthogonal basis of $\mathcal{H}_L$ ($\mathcal{H}_R$) and $\Lambda_\alpha \geq 0$. The Schmidt decomposition is unique up to degeneracies and for a normalized state $|\Psi\rangle$ we find that $\sum_\alpha \Lambda_\alpha^2 = 1$.

An important aspect is that the Schmidt decomposition gives direct insight into the *bipartite entanglement* (i.e., the entanglement between degrees of freedom in $\mathcal{H}_L$ and $\mathcal{H}_R$) of a state. In particular, only one term contributes to the Schmidt decomposition if and only if L and R are not entangled. If more than one term is required in the Schmidt decomposition to express the state, the state is necessarily entangled. The relation between the Schmidt decomposition and the entanglement can be made more concrete. The *re-*

duced density matrix

$$\rho^R = \mathrm{Tr}_L \left(|\psi\rangle\langle\psi| \right) \tag{2}$$

has the Schmidt states $|\alpha\rangle_R$ as eigenstates and the Schmidt coefficients are the square roots of the corresponding eigenvalues, i.e., $\rho^R = \sum_\alpha \Lambda_\alpha^2 |\alpha\rangle_R \langle\alpha|_R$ (equivalently for ρ^L). The reduced density matrix of an entangled (pure) quantum state is the density matrix of a mixed state defined on the subsystem. Thus the *entanglement entropy*, which is defined as the von-Neumann entropy of the reduced density matrix, measures the amount of entanglement. In terms of the Schmidt values, it is given by

$$S = -\sum_\alpha \Lambda_\alpha^2 \log \Lambda_\alpha^2. \tag{3}$$

The entanglement entropy S is a very useful measure to quantify the amount of entanglement in a system for a given bipartition. Finally, the *entanglement spectrum* $\{\epsilon_\alpha\}$ [9] is defined in terms of the spectrum $\{\Lambda_\alpha^2\}$ of the reduced density matrix by $\Lambda_\alpha^2 = \exp(-\epsilon_\alpha)$ for each α.

2 Area Law

A "typical" state in the Hilbert space shows a *volume law*, i.e., the entanglement entropy grows proportionally with the volume of the partitions. In particular, it has been shown in Ref. [10] that a randomly drawn state $|\psi_{\mathrm{random}}\rangle$ from the Hilbert space of a system of N sites with on-site Hilbert space dimension d has an entanglement entropy of $S \approx N/2 \log d - 1/2$ for a bipartition into two parts of $N/2$ sites.

Ground states $|\psi_0\rangle$ of gapped and local Hamiltonians follow instead an *area law*, i.e., the entanglement entropy grows proportionally with the area of the cut [11]. For a cut of an N-site chain as shown in Fig. 1(a) this implies that $S(N)$ is constant for $N \gtrsim \xi$ (with ξ being the correlation length). This can be intuitively understood from the fact that a gapped ground state contains only fluctuations within the correlations length ξ and thus only degrees of freedom near the cut are entangled as schematically indicated in Fig. 1(b). A rigorous proof of the area law in 1D is given in Ref. [12]. In this respect, ground states are very special states and can be found within a very small corner of the Hilbert space as illustrated in Fig. 1(c).

In slightly entangled states, only a relatively small number of Schmidt states contribute significantly. This is demonstrated in Fig. 1(d) by comparing the largest 20 Schmidt values of an area law and a volume law state for a bipartition of an $N = 16$ chain into two half chains.

As an example of an area law state, we consider here the ground state of the transverse field Ising model

$$H = -\sum_n \sigma_n^z \sigma_{n+1}^z + g\sigma_n^x, \tag{4}$$

with σ_n^x and σ_n^z being the Pauli operators and $g > 0$. The $\mathbb{Z}_2$ symmetric model with a phase transition at $g = 1$ has two very simple limits. For $g = 0$, the ground state is twofold degenerate and given by the ferromagnetic product state (symmetry broken) and at $g \to \infty$, the ground state is a product state in which all spins are polarized (symmetric). For intermediate values of g, the ground states are area law type entangled states (except at the critical point). As shown in Fig. 1(d) for a representative example of $g = 1.5$, the ground state has essentially the entire weight contained in a few Schmidt states. Generic states fulfilling the area law show a similar behavior and thus the above observation provides an extremely useful approach to compress quantum states by truncating the Schmidt decomposition. In particular, we can always truncate the Schmidt decomposition at some finite χ such that

$$\left\| |\psi\rangle - \sum_{\alpha=1}^{\chi} \Lambda_\alpha |\alpha\rangle_L \otimes |\alpha\rangle_R | \right\| < \epsilon, \quad \forall \epsilon > 0. \tag{5}$$

This particular property of area law states is intimately related to the MPS representation of 1D quantum states as we will demonstrate in the next section.

The situation is very different for a highly entangled (volume law) random state: All the Schmidt values are roughly constant for all $2^{N/2}$ states and thus only little weight in contained in the 20 dominant states (assuming an equal weight, we find $\sim 1/2^{N/2}$ per Schmidt state).

3 Matrix Product States

A generic quantum state $|\Psi\rangle$ on a chain with N sites can be written in the following MPS form [13, 14, 15]:

$$|\Psi\rangle = \sum_{j_1,\ldots,j_N} A^{[1]j_1} A^{[2]j_2} \ldots A^{[N]j_N} |j_1, \ldots, j_N\rangle. \tag{6}$$

Here, $A^{[n]j_n}$ is a $\chi_{n-1} \times \chi_n$ dimensional matrix and $|j_n\rangle$ with $j_n = 1, \ldots, d$ is a basis of local states at site n. We call the indices of the matrices "bond" indices. The matrices at the boundary, i.e., $n = 1$ and $n = N$, are vectors,

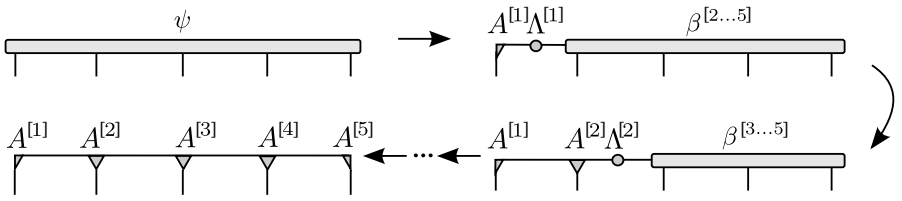

Figure 2: Iterative conversion of a state $|\psi\rangle$ given by a rank-N tensor $\psi_{i_1,\ldots,i_N}$ using successive Schmidt decompositions in a diagrammatic representations. The horizontal lines represent the bond (Schmidt indices) $\alpha, \beta, \gamma, \ldots$ and the vertical lines the physical indices $j_n \in \{1, \ldots, d\}$. Connected lines between tensors denote summation over the corresponding indices (see text for details).

that is $\chi_0 = \chi_N = 1$, such that the matrix product in Eq. (6) produces a number. The superscript $[n]$ denotes the fact that for a generic state, each site is represented by a different set of matrices.

In order to provide some intuition for the structure of MPS, we demonstrate how to transform a generic quantum state

$$|\psi\rangle = \sum_{j_1,j_2,\ldots,j_N} \psi_{j_1,j_2,\ldots,j_N} |j_1, j_2, \ldots j_N\rangle \tag{7}$$

into an MPS. This can be done exactly by performing successively Schmidt decompositions as shown diagrammatically in Fig. 2. This diagrammatic representation, in which a rank-N tensor is represented by a symbol with N legs, is very useful for representing tensor networks and related algorithms. Connecting the legs among tensors symbolizes a tensor contraction, i.e., summing over the relevant indices.

We start by performing a Schmidt decomposition Eq. (1) of the state $|\psi\rangle$ into the first site and the rest such that

$$|\psi\rangle = \sum_{\alpha_1=1}^{d} \Lambda^{[1]}_{\alpha_1} |\alpha_1\rangle_{[1]} |\alpha_1\rangle_{[2,\ldots,N]}. \tag{8}$$

The states $|\alpha_1\rangle_{[1]}$ and $|\alpha_1\rangle_{[2,\ldots,N]}$ form an orthogonal basis for the left and right part, respectively. The first matrix $A^{[i]j_1}_{\alpha_1}$ in the MPS is the matrix relating the left Schmidt states $|\alpha_1\rangle_{[1]}$ with the local states $|j_1\rangle$ (describing the local states on the first site) and is given by $A^{[1]j_1}_{\alpha_1} = \langle j_1|\alpha_1\rangle_{[1]}$. The

resulting mixed representation of the state reads

$$|\psi\rangle = \sum_{j_1=1}^{d} \sum_{\alpha_1=1}^{d} A_{\alpha_1}^{[1]j_1} \Lambda_{\alpha_1}^{[1]} |j_1\rangle |\alpha_1\rangle_{[2,\ldots N]}. \tag{9}$$

Next we proceed to the next bond and perform a Schmidt decomposition of the state such that

$$|\psi\rangle = \sum_{\alpha_2=1}^{d^2} \Lambda_{\alpha_2}^{[2]} |\alpha_2\rangle_{[1,2]} |\alpha_2\rangle_{[3,\ldots,N]}. \tag{10}$$

The second matrix $A_{\alpha_1\alpha_2}^{[2]j_2}$ then relates the mixed basis states $|\alpha_1\rangle_{[1]}|j_2\rangle$ with the left Schmidt states $|\alpha_2\rangle_{[1,2]}$ and is given by $A_{\alpha_1\alpha_2}^{[2]j_2} = \left[\langle\alpha_1|_{[1]}\langle j_2|\right] |\alpha_2\rangle_{[1,2]}$. The resulting mixed representation of the state reads

$$|\psi\rangle = \sum_{\alpha_1=1}^{d} \sum_{\alpha_2=1}^{d^2} \sum_{j_1,j_2=1}^{d} A_{\alpha_1}^{[1]j_1} A_{\alpha_1\alpha_2}^{[2]j_2} \Lambda_{\alpha_2}^{[2]} |j_1, j_2\rangle |\alpha_2\rangle_{[3,\ldots,N]}. \tag{11}$$

This procedure can now be continued until reaching the right end of the chain. We choose the last matrix $A^{[N]j_n}$ to relate the states $\Lambda_{\alpha_N}|\alpha_n\rangle_{[N]}$ to the local basis $|j_n\rangle$. Then it is easy to see that we finally arrive at a representation of the state that has exactly the form Eq. (6).

The caveat is that the matrix dimension increases exponentially as we proceed toward the center of the chain. However, we can make an approximation by neglecting the Schmidt states that have a very small Schmidt values. For the ground state of the Ising model discussed above, we can find a very good approximation of the ground state as MPS by keeping only a maximal bond dimension of $\sim$20 with a truncation error that is of the order of the machine precision (independent of the system size). The same picture can be generalized to all states that fulfill an area law. On more general grounds it had been proven that ground states of one dimensional gapped systems can be efficiently approximated by an MPS [16, 17].

3.1 Canonical form

The representation Eq. (6) is not unique as an MPS with the transformed matrices

$$\tilde{A}^{[n]i_n} = X_{n-1} A^{[n]i_n} X_n^{-1} \tag{12}$$

represents the same state, where the X_n are $\chi_n \times \chi_n$ matrices. In the following, we will show how to fix this degree of freedom by introducing a

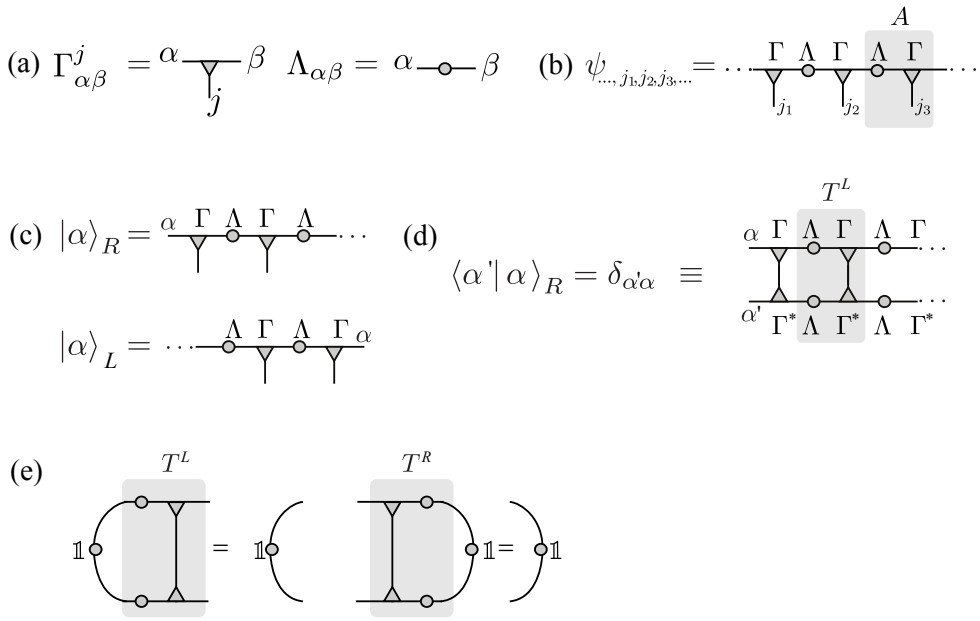

Figure 3: (a): Diagrammatic representation of the tensors Γ and Λ. (b): MPS formed by the tensors Γ and Λ. (c): Definition of the right Schmidt basis states with respect to a partition on a bond with index α. (d): Condition for the MPS to be in the canonical form. The transfer matrix T^L of (16) has been shaded. The upside-down triangles are the complex conjugate of the Γ tensors. (e): If the state is in canonical form, then the dominant left eigenvector of T^L is the "identity matrix" with eigenvalue equal to 1. A similar condition applies for the right transfer matrix T^R.

convenient *canonical* form of the MPS in which the bond index corresponds to the Schmidt decomposition.

Without a loss of generality, we write the matrices $A^{[n]j_n}$ as a product of $\chi_{n-1} \times \chi_n$ matrices $\Gamma^{[n]j_n}$ and positive, real, square diagonal matrices $\Lambda^{[n]}$,

$$|\Psi\rangle = \sum_{j_1,\ldots,j_N} \Gamma^{[1]j_1}\Lambda^{[1]}\Gamma^{[2]j_2}\Lambda^{[2]}\ldots\Lambda^{[N-1]}\Gamma^{[N]j_N}|j_1,\ldots,j_N\rangle, \tag{13}$$

as pictorially illustrated in Figs. 3(a) and 3(b). Let us now motivate the particular choice (13) for the MPS form. The freedom of choosing the MPS can be used to define a "canonical form" of the MPS, following Ref. [18, 19]. As we will see later on, the canonical form has several very useful features. Any bond n defines a bipartition of the system into sites $L = \{1,\ldots,n\}$ and $R = \{n+1,\ldots,N\}$ to the left and right of the bond. From the form of the

MPS, we can define a set of χ_n wave functions $|\alpha\rangle_{[1,\ldots,n]}$ and $|\alpha\rangle_{[n+1,\ldots,N]}$ to the left/right of the bond [see Fig. 3(c)] such that state takes the form

$$|\psi\rangle \;\; = \sum_{\alpha=1}^{\chi} \Lambda_{\alpha}^{[n]} |\alpha\rangle_{[1,\ldots,n]} \otimes |\alpha\rangle_{[n+1,\ldots,N]}. \tag{14}$$

The wave functions $|\alpha\rangle_{L/R}$ are formed by multiplying all matrices to the left and right, respectively. The MPS representation $\{\Gamma^{[1]}, \Lambda^{[1]}, \ldots, \Gamma^{[N]}\}$ is in canonical form if: *For every bond, the set of Schmidt states along with* $\Lambda^{[n]}$ *form a Schmidt decomposition of* Ψ. In other words we must have $\langle\alpha'|\alpha\rangle_{[1,\ldots,n]} = \delta_{\alpha'\alpha}$ and $\langle\alpha'|\alpha\rangle_{[n+1,\ldots N]} = \delta_{\alpha'\alpha}$, along with $\sum(\Lambda_{\alpha}^{[n]})^2 = 1$ on every bond. For finite systems, a generic MPS can be transformed into canonical form by successively orthogonalizing the bonds starting from either the left or right end of the chain [8]. A great advantage of the canonical form is that local expectation values can be evaluated by only contracting the tensors locally by using the orthogonality. Note that the MPS form we obtained above by applying successively Schmidt decomposition provides naturally the canonical form with $A^{[n]j_n} = \Lambda^{[n-1]}\Gamma^{[n]j_n}$.

3.2 Infinite matrix product states

For infinite ($N \to \infty$) and translationally invariant systems, the set of matrices on any given site becomes the same, that is $\Gamma^{[n]j} = \Gamma^j$ and $\Lambda^{[n]} = \Lambda$ for all integers n. Computing the overlaps $\langle\alpha'|\alpha\rangle_R$ would appear to require an infinite tensor contraction. For an infinite MPS, the orthogonality condition can be conveniently expressed in terms of the *transfer matrix* T^R [illustrated in Fig. 3(d)] defined as

$$T^R_{\alpha\alpha';\beta\beta'} \;\; = \sum_j \Gamma^j_{\alpha\beta} \left(\Gamma^j_{\alpha'\beta'}\right)^* \Lambda_\beta \Lambda_{\beta'}, \tag{15}$$

where "*" denotes complex conjugation [19]. The transfer matrix T^R relates the overlaps defined on bond n with overlaps defined on bond $n+1$. Given that the right basis states $|\beta\rangle_R^{[n+1]}$ on bond $n+1$ are orthonormal, the states $|\alpha\rangle_R^{[n]}$ on bond n will also be orthonormal if T has a dominant *right* eigenvector $\delta_{\beta\beta'}(= \mathbb{1})$ with eigenvalue $\eta = 1$, as illustrated in Fig. 3(e). For the left set of states we define an analogous transfer matrix T^L,

$$T^L_{\alpha\alpha';\beta\beta'} \;\; = \sum_j \Lambda_\alpha \Lambda_{\alpha'} \Gamma^j_{\alpha\beta} \left(\Gamma^j_{\alpha'\beta'}\right)^* \tag{16}$$

which must have a *left* eigenvector $\delta_{\alpha\alpha'}$ with $\eta = 1$. These eigenvector criteria are clearly necessary conditions for all bonds to be canonical; in fact, assuming in addition that $\eta = 1$ is the dominant eigenvalue, they are sufficient. The correlation functions in an MPS generically take the form of a

sum of exponentials, with the slowest decaying exponential determined by the second largest (in terms of absolute value) eigenvalue ϵ_2 of the transfer matrix. We define the correlation length of the MPS as

$$\xi = -\frac{1}{\log|\epsilon_2|}, \tag{17}$$

which is readily obtained using a sparse algorithm to find the eigenvalues of the transfer matrix. A state is called *pure* if the dominant eigenvalue is unique and *mixed* if it is degenerate. In the following discussions, we will always assume that the state is *pure* (in fact every mixed state can be uniquely decomposed into pure ones). An algorithm to explicitly transform an arbitrary infinite MPS to the canonical form involves diagonalizing the two transfer matrices T^R and T^L and is given in Ref. [20]. If the infinite MPS is not translational invariant with respect to a one-site unit cell, all the above can be simply generalized by considering a unit-cell of L sites which repeats itself, e.g., in the case of a two site unit cel, the tensors are given by

$$\begin{aligned} \Gamma^{[2n]} &= \Gamma^A, & \Lambda^{[2n]} &= \Lambda^A, \\ \Gamma^{[2n+1]} &= \Gamma^B, & \Lambda^{[2n+1]} &= \Lambda^B, \end{aligned} \tag{18}$$

for $n \in \mathbb{Z}$. Reviews of MPSs as well as the canonical form can be found in Refs. [21, 20, 19].

The infinite MPS representation in the canonical form has a number of important advantages. First, using the properties of the transfer matrices [Fig. 3(e)], it is very convenient to evaluate local expectation values as well as correlation functions. Second, with the help of efficient algorithms such as the *infinite time evolving block decimation* (iTEBD) [19] or *infinite density matrix renormalization group method* (iDMRG) [22], the ground state of a given Hamiltonian can be found in the thermodynamic limit. A discussion of the two algorithms using the same notation as used in these notes can be found in Ref. [23].

3.3 Examples of infinite MPS

To become more familiar with the infinite MPS representation, it is instructive to consider a few concrete examples.

(1) Neel state. The state $|\ldots\uparrow\downarrow\uparrow\downarrow\ldots\rangle$ is a product state with a bond dimension $\chi = 1$ and a local Hilbert space of $d = 2$. The infinite MPS representation is given by

$$\begin{aligned} \Gamma^{[2n],\uparrow} &= \Gamma^{[2n+1],\downarrow} &&= 1 \\ \Gamma^{[2n],\downarrow} &= \Gamma^{[2n+1],\uparrow} &&= 0 \\ \Lambda^{[2n]} &= \Lambda^{[2n+1]} &&= 1. \end{aligned}$$

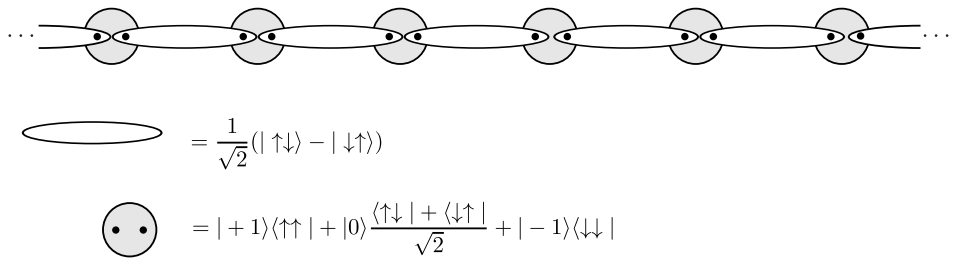

Figure 4: Diagrammatic representation of the AKLT states. The $S = 1$ sites (grey circles) are decomposed into two $S = 1/2$ that are forming a singlet with the neighboring site (ellipsoids).

Note that since the state is a simple product state, the matrices are actually simply complex numbers. It is easy to see that a contraction of the infinite MPS yields the desired Neel state. Furthermore, the corresponding transfer matrices trivially obey the conditions for the canonical form.

(2) Spin-1 AKLT state. Affleck, Kennedy, Lieb, and Tasaki (AKLT) constructed an $S = 1$ Hamiltonian for which the ground state has valence bonds between all neighboring sites (see Fig. 4) [24]. The AKLT Hamiltonian consists of a sum of projectors and reads

$$H = \sum_j \vec{S}_j \vec{S}_{j+1} + \frac{1}{3}(\vec{S}_j \vec{S}_{j+1})^2, \tag{19}$$

where $\vec{S}$ are the spin-1 operators. The ground state in the thermodynamic limit is unique and has a simple ($\chi = 2$) infinite MPS representation

$$\Gamma^{[n],-1} = \sqrt{\frac{4}{3}}\sigma^+, \; \Gamma^{[n],0} = -\sqrt{\frac{2}{3}}\sigma^z, \; \Gamma^{[n],1} = -\sqrt{\frac{4}{3}}\sigma^- \tag{20}$$

$$\Lambda^{[n]} = \sqrt{\frac{1}{2}} \begin{pmatrix} 1 & 0 \\ 0 & 1 \end{pmatrix}. \tag{21}$$

The state can be shown to be in the canonical form by diagonalizing the corresponding left and right transfer matrices.

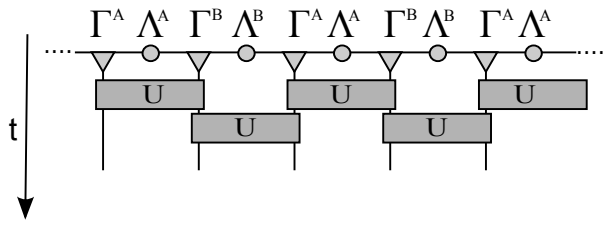

Figure 5: In iTEBD each time step δt of a time evolution is approximated using a Trotter-Suzuki decomposition, i.e., the time evolution operator is expressed as a product of unitary two-site operators.

4 Algorithms

4.1 Infinite Time Evolving Block Decimation (iTEBD)

In the iTEBD algorithm, we are interested in evaluating the time evolution of a quantum state:

$$|\psi(t)\rangle = U(t)|\psi(0)\rangle. \tag{22}$$

The time evolution operator U can either be $U(t) = \exp(-iHt)$ yielding a real time evolution, or an imaginary time evolution $U(\tau) = \exp(-H\tau)$. The latter is used to find ground states of the Hamiltonian H through the relation

$$|\psi_{\mathrm{GS}}\rangle = \lim_{\tau\to\infty} e^{-\tau H}|\psi_0\rangle. \tag{23}$$

To achieve this, one makes use of the Trotter-Suzuki decomposition, which approximates the exponent of a sum of operators, with a product of exponents of the same operators. For example, the first order expansion reads

$$e^{(V+W)\delta} = e^{V\delta}e^{W\delta} + \mathcal{O}(\delta^2). \tag{24}$$

Here V and W are operators, and δ is a small parameter. The second order expansion similarly reads

$$e^{(V+W)\delta} = e^{V\delta/2}e^{W\delta}e^{V\delta/2} + \mathcal{O}(\delta^3). \tag{25}$$

To make use of these expressions, we assume that the Hamiltonian is a sum of two-site operators of the form $H = \sum_n h^{[n,n+1]}$ and decompose it as a sum

$$\begin{aligned} H &= H_{\mathrm{odd}} + H_{\mathrm{even}} \\ &= \sum_{n\ \mathrm{odd}} h^{[n,n+1]} + \sum_{n\ \mathrm{even}} h^{[n,n+1]}. \end{aligned} \tag{26}$$

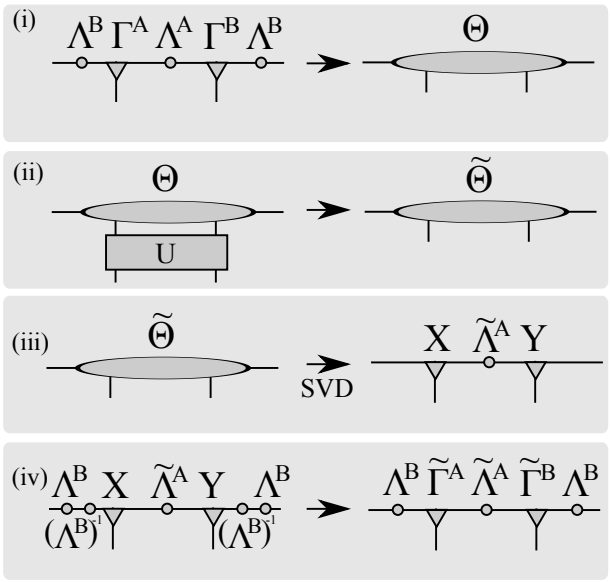

Figure 6: The iTEBD update scheme for a unitary two-site transformation of a two-site unit cell MPS in canonical form (see Sec. 4.1 for details).

Each term H_{odd} and H_{even} consists of a sum of commuting operators.

We now divide the time into small time slices $\delta t \ll 1$ (the relevant time scale is in fact the inverse gap) and consider a time evolution operator $U(\delta t)$. Using, as an example, the first order decomposition (24), the operator $U(\delta t)$ can be expanded into products of two-site unitary operators

$$U(\delta t) \approx \left[\prod_{n \text{ odd}} U^{[n,n+1]}(\delta t)\right] \left[\prod_{n \text{ even}} U^{[n,n+1]}(\delta t)\right], \tag{27}$$

where

$$U^{[n,n+1]}(\delta t) = e^{-i\,\delta t\, h^{[n,n+1]}} \tag{28}$$

This decomposition of the time evolution operator is shown pictorially in Fig. 5. One notices that even if the underlying system has a translation invariance of one site, the decomposition breaks this temporarily into a two site translation symmetry. Therefore, one needs to keep at least two sets of matrices Γ^A, Λ^A and Γ^B, Λ^B. The successive application of these two-site unitary operators to an MPS is the main part of the algorithm.

Local unitary updates of an MPS. One of the advantages of the MPS representation is that local transformations can be performed efficiently.

Moreover, the canonical form discussed above is preserved if the transformations are unitary.[18]

A one-site unitary U simply transforms the tensors Γ of the MPS

$$\tilde{\Gamma}^{j}_{\alpha\beta} = \sum_{j'} U^{j}_{j'} \Gamma^{j'}_{\alpha\beta}. \tag{29}$$

If we consider an infinite, translational invariant MPS, this transformations implies the application of the unitary to *all* equivalent sites simultaneously. In such case the entanglement of the wave-function is not affected and thus the values of Λ do not change.

The update procedure for a two-site unitary transformation acting on two neighboring sites is shown in Fig. 6. We focus on an update of an AB bond between two neighboring sites n and $n+1$ for an MPS with a unit cell of size $N = 2$. The inequivalent BA bonds are updated similarly by simply exchanging A and B. The generalization to an N-site unit cell is straightforward. We first find the wave function in the basis spanned by the left Schmidt states on bond $n-1:n$, the 1-site Hilbert space of sites n and $n+1$, and the right Schmidt states on bond $n+1:n+2$, which together form an orthonormal basis $\{|\alpha_{n-1}\rangle_L, |j_n\rangle, |k_{n+1}\rangle, |\gamma_{n+1}\rangle_R\}$. Calling the wave function coefficients Θ, the state is expressed as

$$|\psi\rangle = \sum_{\alpha,j,k,\gamma} \Theta^{jk}_{\alpha\gamma} |\alpha_{n-1}\rangle_L |j_n\rangle |k_{n+1}\rangle |\gamma_{n+1}\rangle_R. \tag{30}$$

Using the definitions of $|\alpha\rangle_{L/R}$ shown in Fig. 3(b), Θ is given by

$$\Theta^{jk}_{\alpha\gamma} = \sum_{\beta} \Lambda^{B}_{\alpha} \Gamma^{A,j}_{\alpha\beta} \Lambda^{A}_{\beta} \Gamma^{B,k}_{\beta\gamma} \Lambda^{B}_{\gamma}. \tag{31}$$

Writing the wave function in this basis is useful because it is easy to apply the two-site unitary in step (ii) of the algorithm:

$$\tilde{\Theta}^{jk}_{\alpha\gamma} = \sum_{j'k'} U^{jk}_{j'k'} \Theta^{j'k'}_{\alpha\gamma}. \tag{32}$$

Next we have to extract the new tensors $\tilde{\Gamma}^A, \tilde{\Gamma}^B$ and $\tilde{\Lambda}^A$ from the transformed tensor $\tilde{\Theta}$ in a manner that preserves the canonical form. We first 'reshape' the tensor $\tilde{\Theta}$ by combining indices to obtain a $d\chi \times d\chi$ dimensional matrix $\Theta_{j\alpha;k\gamma}$. Because the basis $|\alpha_{n-1}\rangle_L |j_n\rangle$ is orthonormal, as for the right, it is natural to decompose the matrix using the singular value decomposition (SVD) in step (iii) into

$$\Theta_{j\alpha;k\gamma} = \sum_{\beta} X_{j\alpha;\beta} D_{\beta} Y_{\beta;k\gamma}, \tag{33}$$

where X, Y are isometries and D is a diagonal matrix. The isometry X relates the new Schmidt states $|\beta_n\rangle_L$ to the combined bases $|\alpha_{n-1}\rangle_L|j_n\rangle$. Analogously, the Schmidt states for the right site are obtained from the matrix Y. Thus the diagonal matrix D contains precisely the Schmidt values of the transformed state, i.e., $\tilde{\Lambda}^A = D$. The new tensors $\tilde{\Gamma}^A, \tilde{\Gamma}^B$ can be extracted directly from the matrices X, Y using the old matrices Λ^B and the definition of Θ in Eq. (31). In particular we obtain the new tensors in step (iv) by

$$\tilde{\Gamma}^{A,j}_{\alpha\beta} = (\Lambda^B)^{-1}_{\alpha} X_{j\alpha;\beta}, \tag{34a}$$

$$\tilde{\Gamma}^{B,j}_{\beta\gamma} = Y_{\beta;k\gamma}(\Lambda^B)^{-1}_{\gamma}. \tag{34b}$$

After the update, the new MPS is still in the canonical form. Note that as in the one-site update, if we apply the algorithm to an MPS, the update is performed simultaneously to all matrices at equivalent bonds. Thus the iTEBD algorithms exploits the translational invariance of the systems by effectively performing an infinite number of parallel updates at each step.

The entanglement at the bond $n, n+1$ has, in the update, changed and the bond dimension increased to $d\chi$. Thus the amount of information in the wave function grows exponentially if we successively apply unitaries to the state. To overcome this problem, we perform an approximation by fixing the maximal number of Schmidt terms to χ. After each step, only the χ most important states are kept, i.e., if we order the Schmidt states according to their size we simply truncate the range of the index β in Eq. (33) to be $1 \ldots \chi$. This approximation limits the dimension of the MPS and the tensors Γ have at most a dimension of $d \times \chi \times \chi$. Given that the truncated weight is small, the normalization conditions for the canonical form will be fulfilled to a good approximation. In order to keep the wave function normalized, one should divide by the norm after the truncation, i.e., divide by $\mathcal{N} = \sqrt{\sum_{i,j,\alpha,\gamma} \left|\Theta^{ij}_{\alpha\gamma}\right|^2}$.

If we perform an imaginary time evolution of the state, the operator U is not unitary and thus it does not conserve the canonical form. It turns out, however, that the successive Schmidt decompositions assure a good approximation as long as the time steps are chosen small enough. One way to obtain very accurate results is to decrease the size of the time steps successively. [19]

The simulation cost of this algorithm scales as $d^3\chi^3$ and the most time consuming part of the algorithm is the SVD in step (iii). If the Hamiltonian has symmetries, we can considerably accelerate this step by explicitly conserving the resulting constants of motion. The anisotropic spin model we study has for example a global $U(1)$ symmetry and conserves the total magnetization. Thus the matrix $\Theta_{i\alpha;j\gamma}$ has a block-diagonal form and the SVD can be performed in each block individually, yielding a considerable speed up. See Refs. [25, 26] for details of an implementation of symmetries

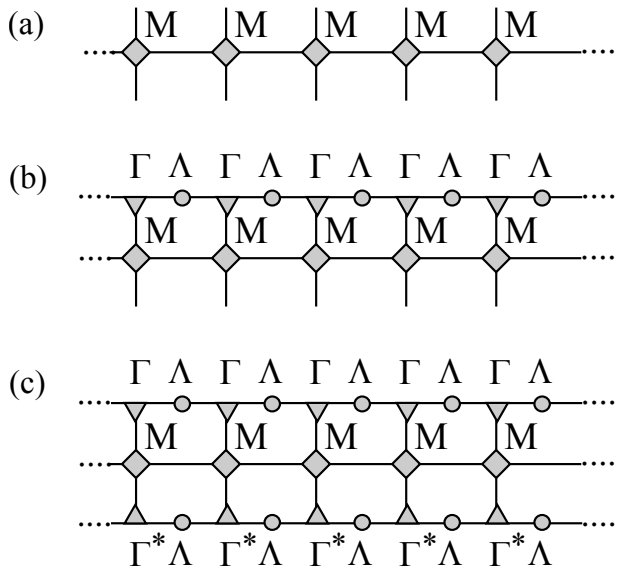

Figure 7: (a) An operator O acting on an entire chain expressed as a matrix product operator. (b) A matrix product operator acting on a matrix product state $O|\psi\rangle$. (c) The expectation value $\langle\psi|O|\psi\rangle$ expressed in an MPO form.

into the algorithm. Numerically, the algorithm can become unstable when the values of Λ become very small since the matrix has to be inverted in order to extract the new tensors in step (iv) of the algorithm. This problem can be avoided by applying a slightly modified version of this algorithm as introduced by Hastings in Ref. [27].

4.2 Matrix-Product Operators

The iDMRG algorithm explained in the next section relies on expressing the Hamiltonian of the system in terms of matrix product operator (MPO). An MPO is a natural generalization of an MPS to the space of operators. An operator in an MPO form, acting on a chain with L sites, is given by

$$O = \sum_{\substack{j_1,\ldots,j_L \\ j'_1,\ldots,j'_L}} \vec{v}_{\text{left}}\, M^{[1]j_1 j'_1}\, M^{[2]j_2 j'_2} \cdots M^{[L]j_L j'_L}\, \vec{v}_{\text{right}} \times |j_1,\ldots,j_L\rangle\langle j'_1,\ldots,j'_L| \,, \tag{35}$$

where $M^{j_n j'_n,}$ are $D \times D$ matrices, and $|j_n\rangle$, $|j'_n\rangle$ represent local states at site n, as before. At the boundaries we initiate and terminate the MPO by the vectors $\vec{v}_{\text{left}}$ and $\vec{v}_{\text{right}}$.

A pictorial representation of an MPO is given in Fig. 7(a). The notation is very similar to the one for an MPS: the horizontal line corresponds to the indices of the virtual dimension and the vertical lines represent the physical states $|j_n\rangle$ (bottom) and $\langle j'_n|$ top. The advantage of the MPO is that it can be applied efficiently to a matrix product state as shown in Fig. 7(b). All local Hamiltonians with only short range interactions can be represented using an MPO of a small dimension D. Let us consider, for example, the MPO of the anisotropic Heisenberg (XXZ) model in the presence of an on-site anisotropy. The Hamiltonian is

$$H_{\mathrm{XXZ}} = J \sum_n \left(S^x_n S^x_{n+1} + S^y_n S^y_{n+1} + \Delta S^z_n S^z_{n+1} + h S^z_n \right), \tag{36}$$

where S^α_n, with $\alpha = x, y, z$, is the α-component of the spin-S operator at site n. Δ is the XXZ anisotropic interaction parameter. Expressed as a tensor product, the Hamiltonian takes the following form:

$$\begin{aligned} H &= S^x \otimes S^x \otimes \mathbb{1} \otimes \cdots \otimes \mathbb{1} + \mathbb{1} \otimes S^x \otimes S^x \otimes \cdots \otimes \mathbb{1} + \ldots \\ &+ S^y \otimes S^y \otimes \mathbb{1} \otimes \cdots \otimes \mathbb{1} + \mathbb{1} \otimes S^y \otimes S^y \otimes \cdots \otimes \mathbb{1} + \ldots \\ &+ \Delta S^z \otimes S^z \otimes \mathbb{1} \otimes \cdots \otimes \mathbb{1} + \ldots \\ &+ [h S^z] \otimes \mathbb{1} \otimes \mathbb{1} \otimes \cdots \otimes \mathbb{1} + \ldots \end{aligned} \tag{37}$$

The corresponding *exact* MPO has a dimension $D = 5$ and is given by

$$M^{[i]} = \begin{pmatrix} \mathbb{1} & 0 & 0 & 0 & 0 \\ S^x & 0 & 0 & 0 & 0 \\ S^y & 0 & 0 & 0 & 0 \\ \Delta S^z & 0 & 0 & 0 & 0 \\ h S^z & S^x & S^y & S^z & \mathbb{1} \end{pmatrix}, \tag{38}$$

with

$$\vec{v}_{\mathrm{left}} = \begin{pmatrix} 0, & 0, & 0, & 0, & 1 \end{pmatrix}, \quad \vec{v}_{\mathrm{right}} = \begin{pmatrix} 1, & 0, & 0, & 0, & 0 \end{pmatrix}^T. \tag{39}$$

By multiplying the matrices (and taking tensor products of the operators), one can easily see that the product of the matrices does in fact yield the Hamiltonian (37). Further details of the MPO form of operators can be found in Refs. [8, 22].

4.3 Infinite Density Matrix Renormalization Group

We now discuss the infinite Density Matrix Renormalization Group (iDMRG) algorithm. Unlike iTEBD, the iDMRG is a variational approach to optimizing the MPS, but the algorithms have many steps in common. One advantage

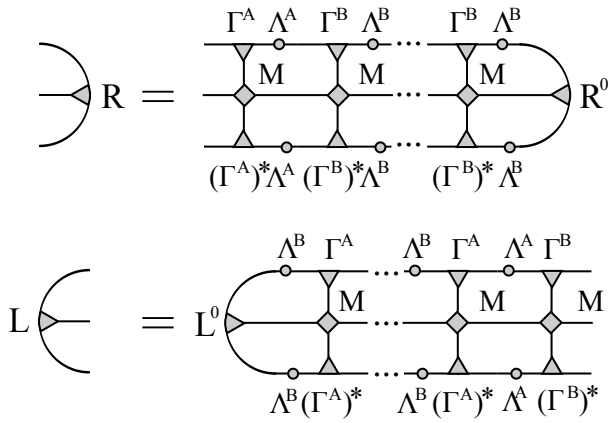

Figure 8: Pictorial representation of a contraction of the left and right environments. The boundaries are initiated by the tensors $R^0_{\alpha\bar{\alpha},a} = \delta_{\alpha\bar{\alpha}}\vec{v}_{\text{right};a}$ and $L^0_{\alpha\bar{\alpha},a} = \delta_{\alpha\bar{\alpha}}\vec{v}_{\text{left};a}$.

of the iDMRG is that it does not rely on a Trotter-Suzuki decomposition of the Hamiltonian and thus applies to systems with longer range interactions. We assume only that the Hamiltonian has been written as an MPO. Secondly, the convergence of the iDMRG method to the ground state is in practice much faster. This is particularly the case if the gap above the ground state is small and the correlation length is long.

The schematic idea for the iDMRG algorithm is as follows (see Fig. 9). Like in iTEBD, the state at each step is represented by an MPS. We variationally optimize pairs of neighboring sites to minimize the ground state energy $\langle\psi|H|\psi\rangle$, while keeping the rest of the chain fixed. To do so, at each step we represent the initial wave function $|\psi\rangle$ using the two site tensor $\Theta^{jk}_{\alpha\gamma}$ (as previously defined in the iTEBD section), project the Hamiltonian into the space spanned by the basis set $|\alpha jk\beta\rangle$, and use an iterative algorithm (e.g. Lanczos) to lower the energy. Repeating this step for each pair, the wave function converges to the ground state. For simplicity, only the details of the algorithm with a unit cell of two sites, A and B, will be described below.

Two-site update algorithm. We start by describing the update of an AB bond between two neighboring sites n and $n+1$ (the update on a BA bond can be performed analogously by exchanging the role of A and B), and return later to the initialization procedure. Step (i) is identical to the first step in the iTEBD method; we contract the tensors for two neighboring

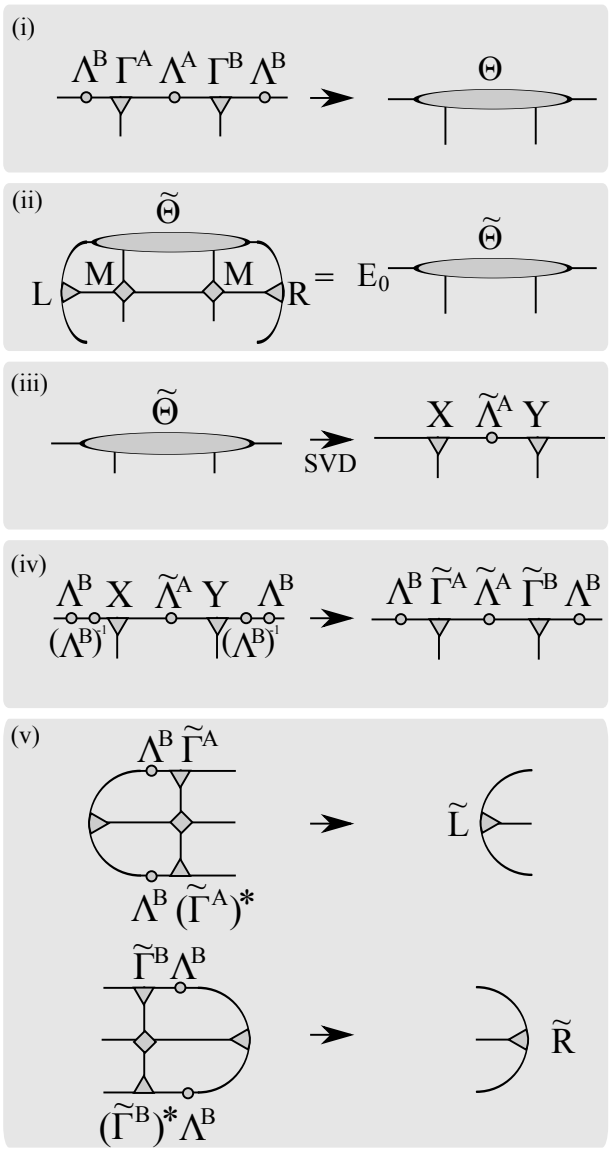

Figure 9: A pictorial representation of an iDRMG iteration step update. Refer to Sec. 4.3 for details.

sites to obtain the initial wave function $\Theta^{jk}_{\alpha\gamma}$. The orthonormal basis $|\alpha j \beta k\rangle$ spans the variational space $|\tilde{\psi}\rangle = \tilde{\Theta}^{jk}_{\alpha\gamma}|\alpha j \beta k\rangle$ of the update, in which we must minimize the energy $E = \langle\tilde{\psi}|H|\tilde{\psi}\rangle$ in order to determine the optimal $\tilde{\Theta}$. Because H is written as an infinite MPO, it appears at first that to evaluate the energy we will have to contract an infinite number of tensors starting from left and right infinity, as illustrated in Fig. 7(c). For the sake

of induction, however, suppose we have already done this contraction on the left through bond $n-1:n$, and on the right through bond $n+1:n+2$. As illustrated in Fig. 8, the result of these contractions can be summarized in two three leg tensors we call the left and right "environments." The left environment $L_{\alpha\bar{\alpha},a}$ has three indices: the MPO index a, and the indices $\alpha, \bar{\alpha}$ corresponding to the bond indices of $|\tilde{\psi}\rangle$ and $\langle\tilde{\psi}|$. Likewise, on the right we have $R_{\gamma\bar{\gamma},c}$. Each bond of the system has a similarly defined environment; for a unit cell of two, we have in total $\{L^A, L^B\}, \{R^A, R^B\}$. These environments are nothing other than the MPO for the Hamiltonian projected into the space of left and right Schmidt states about each bond.

With the environment in hand, we can project the Hamiltonian into the orthonormal basis $|\alpha j\gamma k\rangle$; to minimize the energy of Θ we find the ground state of the $\chi^2 d^2 \times \chi^2 d^2$ "Hamiltonian":

$$H_{\alpha jk\gamma;\bar{\alpha}\bar{j}\bar{k}\bar{\gamma}} = \sum_{a,b,c} L^B_{\alpha\bar{\alpha},a} M^{j,\bar{j}}_{ab} M^{k,\bar{k}}_{bc} R^B_{\gamma\bar{\gamma},c}. \tag{40}$$

To find this ground state, we use an iterative procedure such as Lanczos or Jacobi-Davidson at a cost of $\chi^3 D d^2$ per multiplication, as illustrated in step (ii) of Fig. 9, and obtain an improved guess for the wave function $\tilde{\Theta}$ and energy E_0. By using the initial wave function Θ as the starting vector for the minimization procedure, convergence is typically reached with only a couple of steps. This can be compared to the iTEBD optimization where we obtain a new wave-function $\tilde{\Theta}$ after applying the imaginary time-evolution operator. As with iTEBD, the bond dimension grows as $\chi \to d\chi$, which we must truncate using SVD, shown in step (iii). It is important that the left and right Schmidt basis about any bond remain orthogonal, because we assume $|\alpha j\beta k\rangle$ is an orthogonal basis at each step. Assuming this was the case on bonds of type B, the isometry properties of the SVD matrices X and Y imply that the orthogonality condition holds for the updated Schmidt states defined about the central bond A, and hence will remain so throughout the simulation. At this point, we have improved guesses for the matrices $\tilde{\Gamma}^{A/B}, \tilde{\Lambda}^A$ in step (iv).

The last step is to update the environment. At a minimum, we must update the environments on the bond which we just optimized by simply multiplying new tensors to the left and right as shown in Fig. 9 step (v):

$$\tilde{L}^A_{\beta\bar{\beta},b} = L^B_{\alpha\bar{\alpha},a} \Lambda^B_\alpha \tilde{\Gamma}^A_{\alpha\beta j} M^{j,\bar{j}}_{ab} \Lambda^B_{\bar{\alpha}} (\tilde{\Gamma}^A_{\bar{\alpha}\bar{\beta}\bar{j}})^*, \tag{41a}$$

$$\tilde{R}^A_{\beta\bar{\beta},b} = R^B_{\gamma\bar{\gamma},a} \tilde{\Gamma}^B_{\beta\gamma k} \Lambda^B_\gamma M^{k,\bar{k}}_{ab} (\tilde{\Gamma}^B_{\bar{\gamma}\bar{\beta}\bar{k}})^* \Lambda^B_{\bar{\gamma}}. \tag{41b}$$

This concludes the update on bond AB and we move over by one site, exchanging the roles of A and B, and repeat until convergence is reached.

Initializing the environment. We now return to the problem of initializing the algorithm. The initial MPS can be arbitrary (though it should be in canonical form). A fine choice is a $\chi = 1$ tensor product state which either preserves or breaks the symmetries as desired. To form the initial environment, we suppose when computing the left/right environment that $\hat{H}$ is zero to the left/right of the bond, which is captured by tensors of the form

$$R^{[n]}_{\alpha\bar{\alpha},a} = \delta_{\alpha\bar{\alpha}}\vec{v}_{\text{right};a}, \tag{42a}$$

$$L^{[n]}_{\alpha\bar{\alpha},a} = \delta_{\alpha\bar{\alpha}}\vec{v}_{\text{left};a}, \tag{42b}$$

where the $\vec{v}_{\text{left/right}}$ are the MPO terminal vectors defined in Eq. (35). Referring to Eq. (39) as an example, recall that $\vec{v}_{\text{right}}$ specifies the MPO index such that no further operators will be inserted to its right; likewise, $\vec{v}_{\text{left}}$ indicates no operators have been inserted to its left. Because all terms in the Hamiltonian then act as the identity to the left/right of the bond, the orthogonality of the Schmidt vectors implies that projecting the identity operator into the left/right Schmidt basis trivially gives $\delta_{\alpha\bar{\alpha}}$. When symmetry breaking is expected it is helpful to further initialize the environments by repeatedly performing the iDMRG update *without* performing the Lanczos optimization, which builds up environments using the initial symmetry broken MPS.

Ground state energy from iDMRG. One subtlety of the above prescription lies in the interpretation of the energy E_{GS} obtained during the diagonalization step. Is it the (infinite) energy of the infinite system? Using the initialization procedure just outlined, the Lanczos energy E_{GS} after the first step is the energy of the two-site problem. While we motivated the environments as representing infinite half chains, it is more accurate to assign them a length of 0 after the initialization procedure, and at each optimization step the length of the left/right environment about the central bond increases because a site has been appended. Keeping track of the length $\ell_{R/L}$ of each environment (for a unit cell of two, each grows on alternate steps), we see that the energy E_{GS} corresponds to a system of size $\ell = \ell_L + 2 + \ell_R$. By monitoring the change in E_{GS} with increased ℓ, we can extract the energy per site. This is convenient for problems in which there is no few-site Hamiltonian with which to evaluate the energy.

As for the iTEBD algorithm, we can achieve a considerable speed-up by using the symmetries of the Hamiltonian, which requires assigning quantum numbers to the tensors of the MPO in addition to the MPS.

5 Example Code: iTEBD

The Python code below performs an imaginary time evolution of an MPS to obtain an approximation of the ground state energy. The code can be downloaded at `http://www.pks.mpg.de/~frankp/comp-phys/groundstate.py`.

```
import numpy as np
from scipy.linalg import expm

def itebd(G_list,l_list,U,chi_max):
        "Updates the G and s matrices using U and the TEBD protocol"
        d = G_list[0].shape[0]

        for ibond in [0,1]:
                ia = np.mod(ibond,2); ib = np.mod(ibond+1,2)
                chi1 = G_list[ia].shape[1]
                chi3 = G_list[ib].shape[2]

                # Construct theta
                theta = np.tensordot(np.diag(l_list[ib]),G_list[ia],axes=(1,1))
                theta = np.tensordot(theta,np.diag(l_list[ia],0),axes=(2,0))
                theta = np.tensordot(theta,G_list[ib],axes=(2,1))
                theta = np.tensordot(theta,np.diag(l_list[ib],0),axes=(3,0))

                # Apply U
                theta = np.tensordot(theta,np.reshape(U,(d,d,d,d)),axes=([1,2],[0,1]))

                # SVD
                theta = np.reshape(np.transpose(theta,(2,0,3,1)),(d*chi1,d*chi3))
                X, Y, Z = np.linalg.svd(theta); Z = Z.T
                chi2 = np.min([np.sum(Y>10.**(-10)), chi_max])

                # Truncate
                l_list[ia]=Y[0:chi2]/np.sqrt(sum(Y[0:chi2]**2))
                X=np.reshape(X[:,0:chi2],(d,chi1,chi2))
                G_list[ia]=np.transpose(np.tensordot(np.diag(l_list[ib]**(-1)),X,axes=(1,1)),(1,0,2))
                Z=np.transpose(np.reshape(Z[:,0:chi2],(d,chi3,chi2)),(0,2,1))
                G_list[ib]=np.tensordot(Z,np.diag(l_list[ib]**(-1)),axes=(2,0))

def bond_expectation_value(G_list,l_list,O):
        "Expectation value for a site operator"
        E=[]
        for ibond in range(0,2):
                ia = np.mod(ibond,2); ib = np.mod(ibond+1,2)
                theta = np.tensordot(np.diag(l_list[ib]),G_list[ia],axes=(1,1))
                theta = np.tensordot(theta,np.diag(l_list[ia],0),axes=(2,0))
                theta = np.tensordot(theta,G_list[ib],axes=(2,1))
                theta = np.tensordot(theta,np.diag(l_list[ib],0),axes=(3,0))
                theta_O = np.tensordot(theta,np.reshape(O,(d,d,d,d)),axes=([1,2],[0,1])).conj()
                E.append(np.squeeze(np.tensordot(theta_O,theta,axes=([0,1,2,3],[0,3,1,2]))).item())
        return(E)

######## Define the model and simulation parameters ####################
chi_max=20; delta=0.1; N=2000;d=2; g=0.5

sx = np.array([[0.,1.],[1.,0.]])
sz = np.array([[1.,0.],[0.,-1.]])

H = -np.kron(sz,sz) +  g*np.kron(sx,np.eye(2,2))
U = expm(-delta*H)

################ Initial state : |0000> ###################################
Ga = np.zeros((d,1,1),dtype=float);Ga[0,0,0] = 1.
Gb = np.zeros((d,1,1),dtype=float);Gb[0,0,0] = 1.
G_list = [Ga,Gb]

la = np.zeros(1);la[0] = 1.
lb = np.zeros(1);lb[0] = 1.
l_list = [la,lb]

################ Perform the imaginary time evolution #####################
for step in range(1, N):
        itebd(G_list,l_list,U,chi_max)

print "E=", np.mean(bond_expectation_value(G_list,l_list,H))
```

5.1 Exercises

1. Try out the effect of changing the matrix dimensions χ, the imaginary time step δ, and the number of steps N on the accuracy of the ground state energy.

2. Use the code to sketch the phase diagram by plotting the magnetization m as a function of the transverse field h. How is the convergence near the phase transition? Try different values of χ.

3. Add a function to the code that constructs the transfer matrix T^R. By diagonalizing T^R, you can extract the correlation length ξ from the second largest eigenvalue using Eq. (17). How does ξ behave when approaching the phase transition?

References

[1] Pasquale Calabrese and John Cardy. Entanglement entropy and quantum field theory. *J. Stat. Mech.*, 2004(06):P06002, 2004.

[2] L. Tagliacozzo, T. R. de Oliviera, S. Iblisdir, and J. I. Latorre. Scaling of entanglement support for matrix product states. *Phys. Rev. B*, 78:024410, 2008.

[3] P. Calabrese and A. Lefevre. Entanglement spectrum in one-dimensional systems. *Phys. Rev. A*, 78(032329):032329, 2008.

[4] Frank Pollmann, Subroto Mukerjee, Ari A. M. Turner, and Joel E. Moore. Theory of finite-entanglement scaling at one-dimensional quantum critical points. *Phys. Rev. Lett.*, 102(25):255701, 2009.

[5] Michael Levin and Xiao-Gang Wen. Detecting topological order in a ground state wave function. *Phys. Rev. Lett.*, 96(11):110405, 2006.

[6] Alexei Kitaev and John Preskill. Topological entanglement entropy. *Phys. Rev. Lett.*, 96(11):110404, 2006.

[7] F. Verstraete, J.I. Cirac, and V. Murg. Matrix product states, projected entangled pair states, and variational renormalization group methods for quantum spin systems. *Adv. Phys.*, 57:143, 2008.

[8] Ulrich Schollwöck. The density-matrix renormalization group in the age of matrix product states. *Ann. Phys.*, 326(1):96 – 192, 2011.

[9] H. Li and F. D. M. Haldane. Entanglement spectrum as a generalization of entanglement entropy: Identification of topological order in non-abelian fractional quantum hall effect states. *Phys. Rev. Lett.*, 101:010504, 2008.

[10] Don Page. Average entropy of a subsystem. *Phys. Rev. Lett.*, 71(9):1291–1294, August 1993.

[11] J Eisert, M Cramer, and M B Plenio. Colloquium: Area laws for the entanglement entropy. *Rev. Mod. Phys.*, 82(1):277–306, February 2010.

[12] M. B. Hastings. An area law for one-dimensional quantum systems. *J. Stat. Mech.*, P08024(08), 2007.

[13] M. Fannes, B. Nachtergaele, and R. F. Werner. Finitely correlated states on quantum spin chains. *Comm. Math. Phys.*, 144(3):443–490, 1992.

[14] Stellan Östlund and Stefan Rommer. Thermodynamic limit of density matrix renormalization. *Phys. Rev. Lett.*, 75:3537–3540, Nov 1995.

[15] Stefan Rommer and Stellan Östlund. Class of ansatz wave functions for one-dimensional spin systems and their relation to the density matrix renormalization group. *Phys. Rev. B*, 55:2164–2181, Jan 1997.

[16] Daniel Gottesman and M B Hastings. Entanglement versus gap for one-dimensional spin systems. *New J. Phys.*, 12(2):025002, 2010.

[17] N. Schuch, M. M. Wolf, F. Verstraete, and J. I. Cirac. Entropy scaling and simulability by matrix product states. *Phys. Rev. Lett.*, 100(3):030504, 2008.

[18] G. Vidal, J. I. Latorre, E. Rico, and A. Kitaev. Entanglement in quantum critical phenomena. *Phys. Rev. Lett.*, 90(22):227902, Jun 2003.

[19] G. Vidal. Classical simulation of infinite-size quantum lattice systems in one spatial dimension. *Phys. Rev. Lett.*, 98(070201):070201, FEB 16 2007.

[20] R. Orús and G. Vidal. Infinite time-evolving block decimation algorithm beyond unitary evolution. *Phys. Rev. B*, 78:155117, Oct 2008.

[21] D. Perez-Garcia, F. Verstraete, M.M. Wolf, and J.I. Cirac. Matrix product state representations. *Quantum Inf. Comput.*, 7:401, 2007.

[22] Ian P McCulloch. From density-matrix renormalization group to matrix product states. *J. Stat. Mech.*, P10014(10), 2007.

[23] Jonas A. Kjäll, Michael P. Zaletel, Roger S. K. Mong, Jens H. Bardarson, and Frank Pollmann. Phase diagram of the anisotropic spin-2 xxz model: Infinite-system density matrix renormalization group study. *Phys. Rev. B*, 87:235106, Jun 2013.

[24] I. Affleck, T. Kennedy, E. Lieh, and H. Tasaki. *Phys. Rev. Lett.*, 59:799, 1988.

[25] Sukhwinder Singh, Robert N. C. Pfeifer, and Guifré Vidal. Tensor network decompositions in the presence of a global symmetry. *Phys. Rev. A*, 82:050301, Nov 2010.

[26] Sukhwinder Singh, Robert N. C. Pfeifer, and Guifre Vidal. Tensor network states and algorithms in the presence of a global u(1) symmetry. *Phys. Rev. B*, 83:115125, Mar 2011.

[27] M. B. Hastings. Light-cone matrix product. *J. Math. Phys.*, 50(9):095207, 2009.